Please cite this article in press as: Mukherjee et al., Local magnetic delivery of adeno-associated virus AAV2(quad Y-F)-mediated BDNF gene therapy restores hearing after noise injury, Molecular Therapy (2021), https://doi.org/10.1016/j.ymthe.2021.07.013

Molecular Therapy
Original Article

Local magnetic delivery of adeno-associated virus AAV2(quad Y-F)-mediated BDNF gene therapy restores hearing after noise injury

Subhendu Mukherjee,[1] Maya Kuroiwa,[4] Wendy Oakden,[2] Brandon T. Paul,[3] Ayesha Noman,[1] Joseph Chen,[4] Vincent Lin,[1,4] Andrew Dimitrijevic,[3,4] Greg Stanisz,[2] and Trung N. Le[1,4]

[1]Biological Sciences Platform, Hurvitz Brain Sciences Program, Sunnybrook Research Institute, Toronto, ON M4N 3M5, Canada; [2]Physical Sciences Platform, Sunnybrook Research Institute, Toronto, ON M4N 3M5, Canada; [3]Evaluative Clinical Sciences Platform, Sunnybrook Research Institute, Toronto, ON M4N 3M5, Canada; [4]Department of Otolaryngology Head & Neck Surgery, Faculty of Medicine, University of Toronto, ON M5S 1A1, Canada

Moderate noise exposure may cause acute loss of cochlear synapses without affecting the cochlear hair cells and hearing threshold; thus, it remains "hidden" to standard clinical tests. This cochlear synaptopathy is one of the main pathologies of noise-induced hearing loss (NIHL). There is no effective treatment for NIHL, mainly because of the lack of a proper drug-delivery technique. We hypothesized that local magnetic delivery of gene therapy into the inner ear could be beneficial for NIHL. In this study, we used superparamagnetic iron oxide nanoparticles (SPIONs) and a recombinant adeno-associated virus (AAV) vector (AAV2(quad Y-F)) to deliver brain-derived neurotrophic factor (BDNF) gene therapy into the rat inner ear via minimally invasive magnetic targeting. We found that the magnetic targeting effectively accumulates and distributes the SPION-tagged AAV2(quad Y-F)-BDNF vector into the inner ear. We also found that AAV2(quad Y-F) efficiently transfects cochlear hair cells and enhances BDNF gene expression. Enhanced BDNF gene expression substantially recovers noise-induced BDNF gene downregulation, auditory brainstem response (ABR) wave I amplitude reduction, and synapse loss. These results suggest that magnetic targeting of AAV2(quad Y-F)-mediated BDNF gene therapy could reverse cochlear synaptopathy after NIHL.

INTRODUCTION

Changes in the hearing threshold after noise-induced hearing loss (NIHL) can be temporary or permanent. Permanent NIHL is caused by irreparable damage to cochlear hair cells.[1] On the other hand, although hair cell damage and threshold change recover rapidly in temporary NIHL, studies have shown that moderate noise exposure can destroy synapses and significantly attenuates auditory brainstem response (ABR) wave I amplitude.[2–4] Loss of synapses between inner hair cells (IHCs) and spiral ganglion neurons (SGNs) is one of the main pathologies of NIHL.[5] Clinically, hearing thresholds may recover within days or weeks, and routine audiological examinations may fail to detect this form of damage to cochlear synapses in humans. Thus, this form of hearing loss is known as hidden hearing loss or cochlear synaptopathy.[6]

Studies have suggested that neurotrophins can prevent the noise-mediated degeneration of neuronal elements and thus can be used to treat NIHL.[7–11] It has been shown that transplantation of neurotrophin-secreting olfactory stem cells into the cochlea and application of brain-derived neurotrophic factor (BDNF) on the round window can potentially reduce synaptopathy.[10,12] Mesenchymal stem cell (MSC)-mediated elevation of BDNF in the cochlea has been shown to protect the cochlea against ototoxicity by improving SGN survival.[13] Adeno-associated viruses (AAVs) are widely used to deliver gene therapy in the inner ear. Recombinant AAV vectors are being developed to improve the transduction efficiency of different therapeutic genes in the inner ear.[14]

One of the main challenges in treating inner-ear diseases is determining the best route of delivery. Conventional routes of administration, such as oral and parenteral routes, are often the first-line approach for treating inner-ear diseases, but these approaches can lead to subtherapeutic drug concentration in the inner ear because of the blood-labyrinth barrier.[15] On the other hand, the main obstacle in local drug delivery to the cochlea is its complex and fragile microstructures. In the intratympanic method, drug substances are injected in the middle ear with the aim of passive diffusion through the round window membrane (RWM) to the inner ear. With intracochlear administration, drug substances are directly injected into the cochlea; however, surgery often results in disruption of inner-ear homeostasis leading to possible further physical damage resulting in hearing loss and vertigo.[14] Magnetic targeting of gene therapy is a new and evolving field. Magnetizable nanoparticles are used to deliver and concentrate therapeutic substances in the region of disease safely and easily.[16–21] Very few studies have been done to explore magnetic targeting as a local delivery approach to the inner ear.[22–26] Recently,

Received 5 December 2020; accepted 14 July 2021;
https://doi.org/10.1016/j.ymthe.2021.07.013.

Correspondence: Trung N. Le, Biological Sciences Platform, Hurvitz Brain Sciences Program, Sunnybrook Health Sciences Centre, 2075 Bayview Ave., Room M1 102, Toronto, ON M4N 3M5, Canada.
E-mail: trung.le@sunnybrook.ca

Please cite this article in press as: Mukherjee et al., Local magnetic delivery of adeno-associated virus AAV2(quad Y-F)-mediated BDNF gene therapy restores hearing after noise injury, Molecular Therapy (2021), https://doi.org/10.1016/j.ymthe.2021.07.013

Le et al.[13] successfully used magnetic targeting for systemic delivery of MSCs and superparamagnetic iron oxide nanoparticles (SPIONs) to the inner ear.

We hypothesized that local magnetic targeting is a safe and efficient delivery technique for AAV-mediated BDNF gene therapy to treat NIHL. In our study, we employ local magnetic delivery of the AAV2(quad Y-F) vector into the inner ear to elevate BDNF levels. SPIONs were attached to the virus to facilitate magnetic targeting delivery into the inner ear of a NIHL rat model. Magnetic resonance (MR) imaging (MRI) was used to confirm the distribution of the SPION inside the cochlea. SPION delivery did not cause ototoxicity to the inner ear. Magnetic targeting of AAV2(quad Y-F)-BDNF vectors to the inner ear enhanced BDNF gene expression in the cochlea. That overexpression of the BDNF gene recovers synapses and ABR wave I amplitude after NIHL. These data demonstrated for the first time the ability to deliver gene therapy locally via a minimally invasive, trackable, and effective magnetic targeting technique that can potentially improve hearing performance to treat NIHL.

RESULTS

Efficacy of local magnetic targeting of SPION to inner ear

SPIONs consist of the ferric iron (Fe^{3+}) and ferrous iron (Fe^{2+}) core and have a large magnetic moment, which leads to local magnetic field inhomogeneity and a significant decrease in MRI signal intensity. Hence, SPIONs appear dark on T2-weighted images,[27] allowing their location to be visualized *in vivo*. SPIONs (20 μL) were deposited onto the RWM (left ear) of 6- to 8-week-old rats via a postauricular surgical approach. The SPIONs were targeted inside the inner ear using an external magnet for 30 min, while the right ear is preserved as control. Our MRI results showed SPION localization in the cochlea, vestibule, and semicircular canals of the ear where SPIONs were magnetically targeted locally (Figure 1). Axial and coronal views of the MRIs confirmed that SPION-associated signal loss (dark/black signal) was observably higher in the cochlea of the SPION-treated ear (left ear) compared to the control untreated ear (right ear) (white T2 fluid signal) when using magnetic targeting (Figures 1ib , and 1i d). There was no apparent signal loss due to SPION contrast in the treated left ear compared to the control right ear without magnetic targeting (Figures 1i a, and 1i c). Sagittal view of the left ear provided a direct comparison between magnetically targeted and untargeted groups, showing a higher SPION contrast (darker signal) in the magnetically targeted ear (Figures 1i e, and 1i f). A three-dimensional MRI view of the inner ear showed a white fluid signal loss, indicative of the presence of SPION contrast (black signal), in basal and mid-turn of the cochlea, vestibule, and horizontal semicircular canal (HSCC) of the magnetically targeted ear (Figures 1i g, and 1i h). Additionally, quantification of the MRI signal in various regions of interest (ROIs; ROI 1: basal turn, ROI 2 and ROI 3: mid-turn, ROI 4 and ROI 5: apex) (Figure 1ii a) was performed by obtaining a relative signal intensity ratio of the treated ear over the control ear for each region. A mixed analysis of variance (ANOVA) was used to compare the treated and control ears across ROIs and indicated a significant group by ROI interaction ($F(2.43, 12.15) = 9.46$, $p = 0.002$, Greenhouse-Geisser corrected) suggesting that a change in relative signal ratio depended on the cochlear region (Figure 1ii b). Significantly more SPION contrast was delivered to the basal turn as compared to the mid-turn and apex ($p < 0.015$) in the magnetic targeting group, whereas there was no difference between the apex and mid-turn ($p > 0.32$). No differences were found between cochlear regions in the group without magnetic targeting ($p > 0.18$). Finally, the signal intensity was higher in the group without magnetic targeting versus the magnetic targeting group at the basal turn ($p < 0.0008$), and this difference was marginally significant at the mid-turn and apex ($p < 0.06$).

Magnetic targeting of SPIONs has no adverse effect on the inner-ear hearing function

After confirming that magnetic targeting can be used to deliver SPIONs to the inner ear, we assessed for adverse effects of this procedure on the hearing thresholds of our animals. The results showed no significant changes in ABR threshold at any of the frequencies examined (4 kHz, 8 kHz, 16 kHz, 24 kHz, and 32 kHz) in the treated ear at 2 weeks and 4 weeks after surgery/delivery (Figures 2i a, and 2i b). We also did not find any significant changes in ABR threshold value between male and female rats in the control and SPOIN (with magnetic targeting)-treated groups. However, we found that hearing thresholds were lower (better hearing) in female rats at 8 kHz (at 4-week time point) and 16 kHz and 32 kHz frequencies, mainly in control ears (Figure S1i). Our result suggested that magnetic targeting of SPION did not have any adverse effect on the normal hearing of male or female rats.

To further assess the effect of magnetic delivery of SPIONs to the inner-ear microstructure, we examined the histology of the hair cells and hair cell stereocilia bundles in both treated and control ears. Anti-myosin VIIa was used to label hair cells, and phalloidin conjugated to Alexa 488 was used to stain actin filament (Figure 2ii). The results did not show any observable loss of outer hair cells (OHCs), IHCs, and stereocilia bundles in any of the cochlear turns (basal [>20 kHz], mid-turn [8−20 kHz], and apex [<8 kHz]; Figure S1ii) of control and SPION with magnetic targeting-treated rats (Figure 2ii).

AAV2(quad Y-F) efficiently transduced cochlear hair cells

Initially, we tested the hair cell transduction efficiency of AAV2(quad Y-F). Magnetic delivery of 6.06×10^{10} genome-containing (GC) particle of AAV2(quad Y-F)-BDNF-GFP-SPION was performed in rats without noise exposure. SPIONs (20 μL) were tagged with AAV2(quad Y-F) and were deposited onto the RWM (left ear) of 6- to 8-week-old rats via a postauricular surgical approach. The SPIONs were then targeted inside the inner ear using an external magnet near the contralateral ear for 30 min. The rats were sacrificed after 4 weeks, and the cochleae were collected and immunostained for GFP and hair cells (using anti-myosin VI) (Figures 3i−3iii). We found that AAV2(quad Y-F) efficiently transduced both OHCs and IHCs in all three turns of the cochlea (basal turn, mid-turn, and

Please cite this article in press as: Mukherjee et al., Local magnetic delivery of adeno-associated virus AAV2(quad Y-F)-mediated BDNF gene therapy restores hearing after noise injury, Molecular Therapy (2021), https://doi.org/10.1016/j.ymthe.2021.07.013

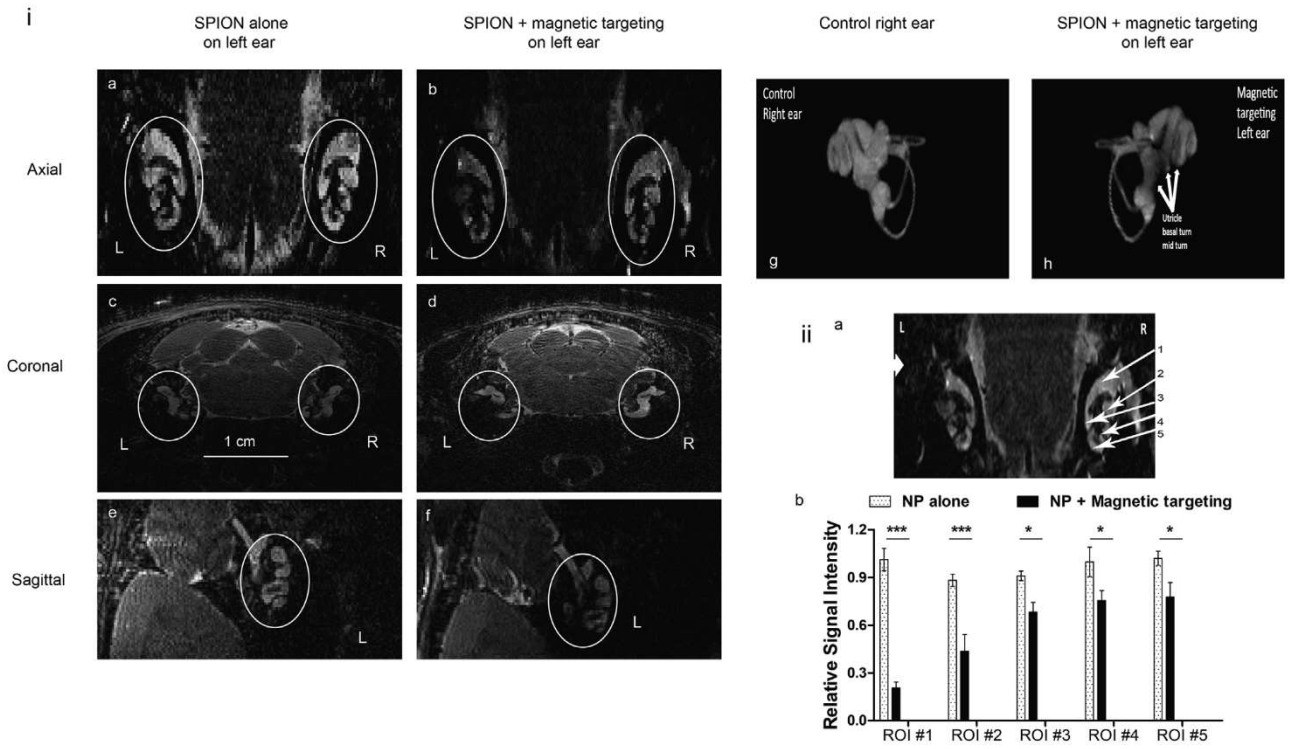

Figure 1. Better distribution of SPION in the inner ear after magnetic targeting

T2- weighted MRIs of rat ears using a 3D RARE sequence after postauricular administration of SPION (nanoparticle [NP]) (i, a-h). For the magnetic targeting group, SPION was targeted inside the inner ear using an external magnet for 30 min. The ears were imaged after the incubation with a magnet was done. Left ear images of the SPION + magnetic targeting group rats show loss of signal intensity due to SPION (the intensity of white fluid signal between the circles in each panel) in the cochlear turns and semicircular canal than that of the right ears (i, b and d). Also, SPION with magnetic targeting left ears showed a better distribution of SPION in the inner ear (i, b, d, and f) than that of the ears that are treated with SPION alone (without magnet) (i, a, c, and e). 3D images of T2-weighted MRI showed more signal loss due to SPION (white arrow) in the cochlear turns and semicircular canal of the left ear than that of the right ears in SPION + magnetic targeting group rats (i, g and h); n = 4 per group. Five random regions of interest (ROIs) were selected in the left ears of SPION with or without magnetic targeting group rats (ii, a), ROI #1 basal turn, ROI #2 and #3 mid-turn, and ROI #4 and #5 apex. The corresponding ROIs were chosen in the control ears. White bars represent the relative signal intensity of SPION alone-treated left ear over control ear (right ear), and black bars represent the relative signal intensity of SPION with magnetic targeting-treated left ear over control ear (ii, b). Decreased signals were observed in ROIs of the SPION + magnetic targeting group than that of the SPION-alone group (ii, b). Better SPION distribution was found in basal turn (ROI #1), mid-turn (ROI #2 and #3), and apex (ROI #4 and #5) of SPION + magnetic targeting group. Bar diagrams indicate mean ± SEM values of relative MRI signal intensity. *$p < 0.05$, **$p < 0.01$, ***$p < 0.001$; n = 4 per group.

apex) when magnetically targeted into the inner ear (Figures 3i, 3i a, 3i d, and 3i g). In contrast, the AAV2(quad Y-F)-BDNF-GFP alone-treated group showed weak GFP expression at the basal turn and poor GFP expression at mid-turn and apex (Figures 3ii, 3ii a, 3ii d, and 3ii g). We did not find any noticeable GFP staining in the untreated control ear (Figures 3iii, 3iii a, 3iii d, and 3iii g)

To confirm the efficiency of AAV2(quad Y-F)-BDNF-GFP-mediated gene delivery in the inner ear, we analyzed the expression level of GFP and BDNF mRNA in the cochlea after magnetic delivery. Both sets of analysis found a main effect of group (for GFP, $F(2,15) = 25.5$, $p < 0.001$; for BDNF, $\chi^2(2) = 6.50$, $p = 0.039$). Post hoc comparisons did not return any significant changes in GFP and BDNF gene expression in the ears that were treated with AAV2(quad Y-F)-BDNF-GFP without magnetic targeting (Figure 3iv; $p > 0.42$). However, AAV2(quad Y-F)-BDNF-GFP-SPION and magnetic targeting-treated ears showed an ~24-fold increase in GFP gene expression and ~7-fold increase in BDNF gene expression in comparison to control ears by 2 weeks of the delivery (Figure 3iv; $p < 0.02$). We also checked the expression level of SRY (sex determining region Y)-box transcription factor 2 (SOX2) mRNA as a marker of the cochlea-specific gene. We did not find any changes in SOX2 expression in control and AAV2(quad Y-F)-BDNF-GFP-SPION and magnetic targeting-treated ears (Figure S2).

Effect of the local magnetic delivery of BDNF gene therapy on cochlear function

To assess the functional effects of the magnetic delivery of BDNF gene therapy to the inner ear, the hearing was measured before and after the gene delivery in a rat model of NIHL. ABR wave I was assessed at threshold (reflecting the function of high spontaneous discharge rate [SR] synapses) and above threshold (i.e., suprathreshold, reflecting the function of low-SR synapses).

Please cite this article in press as: Mukherjee et al., Local magnetic delivery of adeno-associated virus AAV2(quad Y-F)-mediated BDNF gene therapy restores hearing after noise injury, Molecular Therapy (2021), https://doi.org/10.1016/j.ymthe.2021.07.013

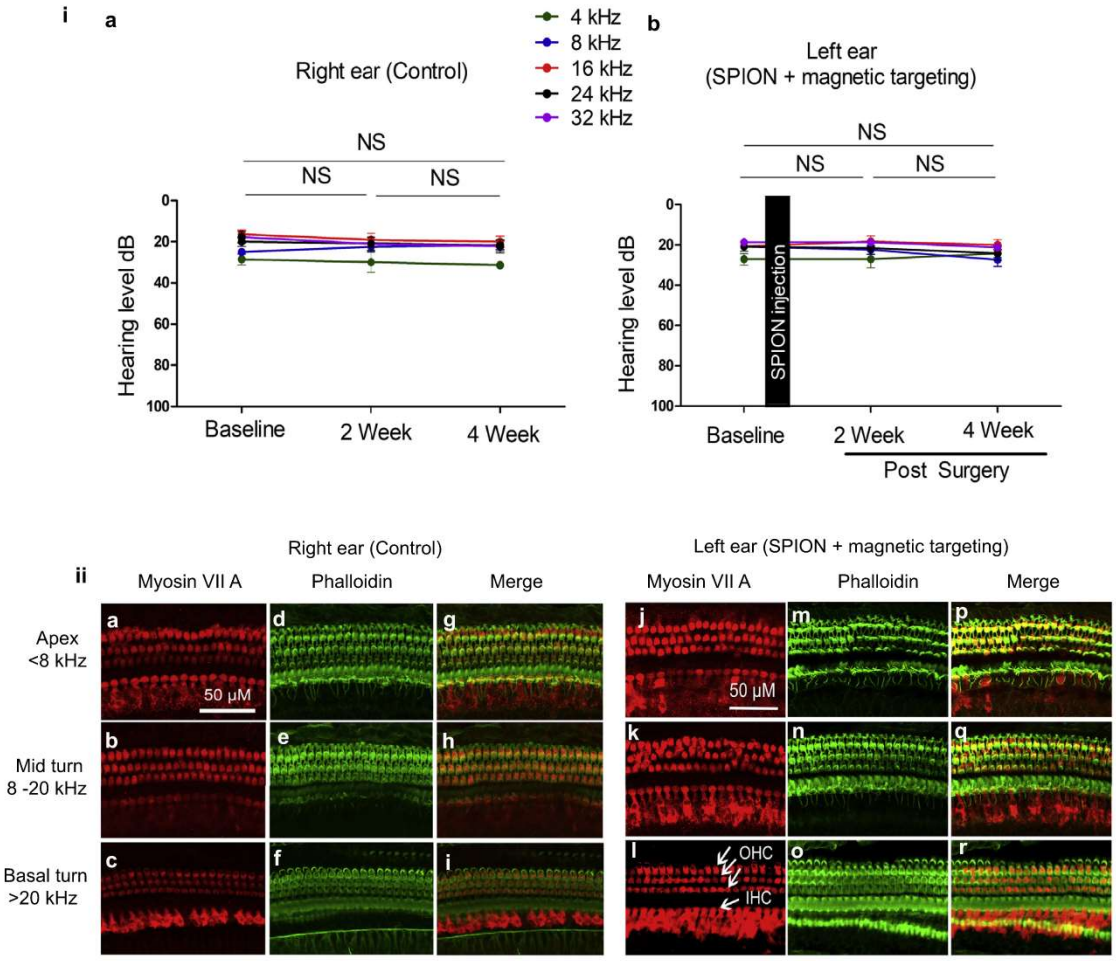

Figure 2. Magnetic targeting of SPION does not have any adverse effect on hearing and hair cells in non-deafened ears

Representative traces of auditory brainstem response (ABR) in control (right) ear (i, a) and SPION (NP) with magnetic targeting-treated (left) ear (i, b) before and after local delivery of SPION, evoked by pure tones at 4 kHz, 8 kHz, 16 kHz, 24 kHz, and 32 kHz. There were no significant changes in ABR absolute threshold at any of the five frequencies in the control ear or SPION with magnetic targeting-treated ear, after 2 weeks and 4 weeks of delivery. The black vertical bar (i, b) indicates the time of SPION administration. Mean ± SEM values of the ABR threshold are shown in the graphs for n = 12 animals (6 male and 6 female animals). (ii) Representative immunostaining images of cochlear hair cells (stained with anti-myosin VIIa, red stain) and hair cell stereocilia bundles (stained with Alexa Fluor 488 phalloidin, green stain) in the organ of Corti of control (ii, a-i) and SPION with magnetic targeting ears (ii, j-r). There were no changes in cochlear hair cells and hair cell stereocilia bundles at any of the three turns of the control and SPION with magnetic targeting-treated ears after 4 weeks of SPION administration. White arrows indicate OHCs and inner hair cells (IHCs). Immunofluorescence (IF) images are representative images of n = 6 animals in each group. Photomicrographs were all taken in the same setting (20× optical zoom) and exposure time.

ABR threshold shifts were calculated by subtracting the pre-noise threshold value from the post-noise value. At first, we checked the effect of the 2-h exposure of an octave band of noise (8–16 kHz) at 110 decibel (dB) sound pressure level (SPL) on the ABR threshold shift in 6- to 8-week-old male and female rats. We found that 2-h exposure to 110 dB SPL noise caused a reversible ABR threshold change in both male and female rats in all four experimental frequencies (4 kHz, 16 kHz, 24 kHz, and 32 kHz). The threshold shift caused by the noise exposure was fully or partially recovered by 4 weeks of the noise exposure in both male and female rats (Figure S3). Interestingly, we found a trend of less noise-induced threshold shift in female rats than male rats, but those changes were not statistically significant. As in our experimental setup, we did not find any significant different effects of noise exposure on the ABR threshold shifts between male and female rats; we combined the male and female rats to analyze the effect of magnetic targeting of AAV2(quad Y-F)-BDNF-SPION on NIHL. Our analysis showed that 2-h exposure to an octave band of noise (8−16 kHz) at 110 dB SPL caused a moderately significant and partially reversible change in the ABR threshold in 6- to 8-week-old Long-Evans rats (for both sexes similarly) (Figures 4i−4iv). In the control ear, at 48-h post-noise exposure, there was an ∼20- to 25-dB threshold shift in high frequency (16 kHz, 24 kHz, and 32 kHz) and a relatively smaller threshold shift (∼10−15 dB) in low frequency (4 kHz). These threshold shifts returned toward the pre-noise value

Please cite this article in press as: Mukherjee et al., Local magnetic delivery of adeno-associated virus AAV2(quad Y-F)-mediated BDNF gene therapy restores hearing after noise injury, Molecular Therapy (2021), https://doi.org/10.1016/j.ymthe.2021.07.013

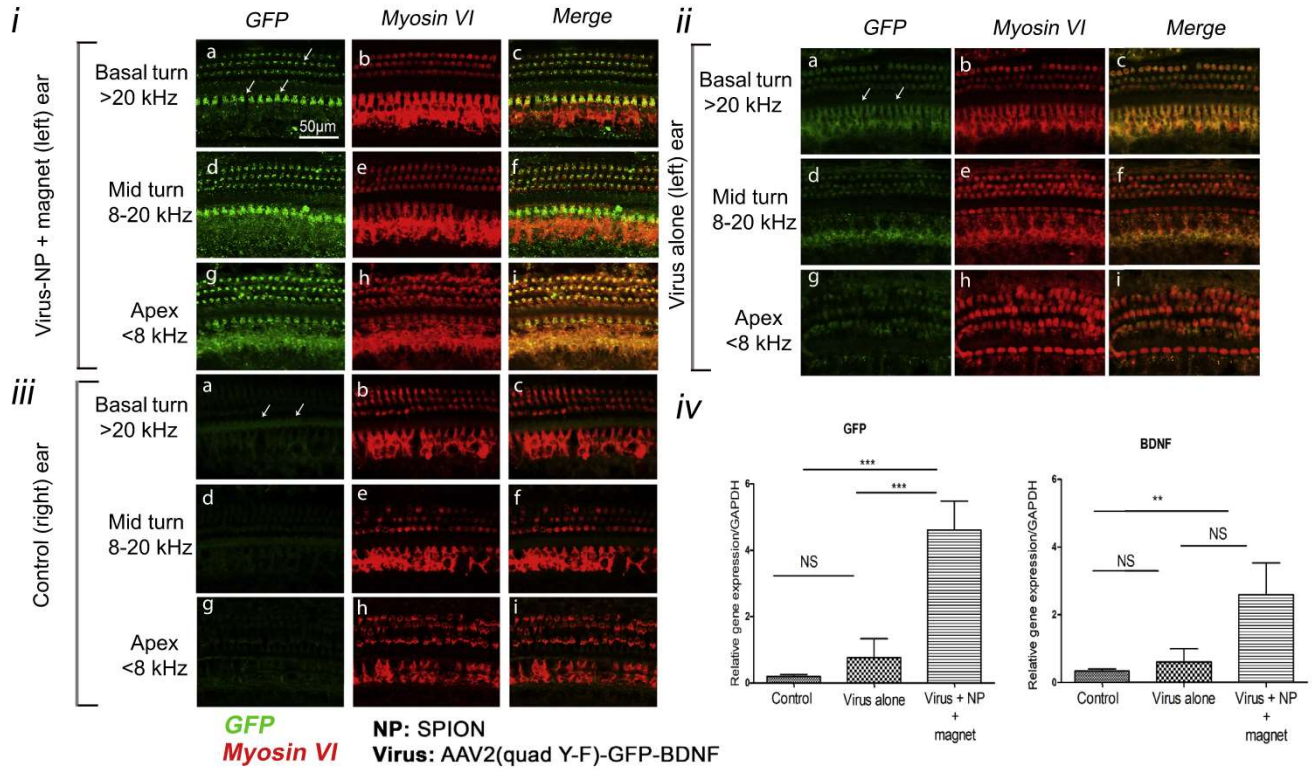

Figure 3. AAV2(quad Y-F) infects cochlear OHCs and IHCs with high efficiency

Representative confocal images of GFP and myosin VI staining in the apex (<8 kHz), mid-turn (8–20 kHz), and basal turn (>20 kHz) of control (iii), AAV2(quad Y-F)-GFP-BDNF (virus alone) (ii), and AAV2(quad Y-F)-GFP-BDNF-SPION (virus-NP)-treated ears (i). AAV2(quad Y-F)-GFP-BDNF (virus) and AAV2(quad Y-F)-GFP-BDNF-SPION (virus-NP) were administered in the left-ear round window niche following a retro-auricular approach at a dose of 6.06×10^{10} CG particles and were targeted to the inner ear using an external magnetic field (for virus-NP group only). In the AAV2(quad Y-F)-GFP-BDNF-SPION group, the IHCs and OHCs were infected with high efficiency throughout the entire cochlea (i, a, d, and g). GFP expression is shown in green (i, a, d, and g; ii, a, d, and g; and iii, a, d, and g), and myosin VI (marker for hair cells) expression is shown in red (i, b, e, and h; ii, b, e, and h; and iii, b, e, and h). Weak GFP staining was observed in the virus-alone group ears (ii), and no noticeable GFP staining was observed in the right (control) ears (iii). Rat cochleae were collected 4 weeks after AAV2(quad Y-F)-GFP-BDNF delivery and were processed for IF. IF data shown are representative of at least 6 independent experiments using different animals. Photomicrographs were taken at the same setting (20× zoom) and exposure time for all pictures. The expression level of GFP and BDNF mRNA in rat cochlea (iv) was significantly enhanced in the AAV2(quad Y-F)-GFP-BDNF-SPION with magnetic targeting (virus-NP) ears than that of the control (right) ears. AAV2(quad Y-F)-GFP-BDNF alone (virus alone) treatment did not show any significant changes in GFP or BDNF gene expression. Rat cochleae were collected 2 weeks after delivering AAV2(quad Y-F)-BDNF-GFP ± SPION and were processed for RT-PCR. Bar diagrams indicate mean ± SEM values of relative gene expression. *$p < 0.05$, **$p < 0.01$, ***$p < 0.001$; $n = 9$ (control), 4 (AAV2(quad Y-F)-GFP-BDNF alone), and 5 (AAV2(quad Y-F)-GFP-BDNF with magnetic targeting) animals.

by 4 weeks, partially for 4, 16, and 32 kHz, and complete recovery for 24 kHz. There was no observed recovery of threshold shift at 2 weeks. Similar patterns were seen in the SPION alone with the magnetic targeting group and the AAV2(quad Y-F)-BDNF-alone (without magnet) group. Interestingly, for the ears that were treated with AAV2(quad Y-F)-BDNF-SPION with magnetic targeting, there was a rapid recovery of threshold shift for all examined frequencies toward the pre-noise value by 2 weeks (Figures 4i–4iv). The recovery was complete and comparable to the pre-noise hearing value by 4 weeks for 24 and 32 kHz (Figures 4iii and 4iv).

These observations were supported in multilevel modeling analyses, indicating a significant interaction of group and time point of testing ($F(9,307.25) = 5.55$, $p < 0.001$). Note that a three-way interaction was not found with frequency, suggesting that there was no evidence that the group-by-time interaction depended on the frequencies tested. Post hoc comparisons revealed that the ears treated with AAV2(quad Y-F)-BDNF-SPION with magnetic targeting had smaller threshold shifts compared to the control SPION with magnet groups at 2 weeks at 16, 24, and 32 kHz ($p < 0.043$). Thresholds were also lower for the AAV2(quad Y-F)-BDNF-SPION without magnet group at 24 kHz and 2 weeks compared to the control group ($p = 0.011$). No other contrasts were statistically significant.

For control ears, we found that 2-h exposure to 110 dB SPL resulted in an ~15- to 20-dB shift in the distortion product (DP) otoacoustic emission (OAE) threshold after 48 h in the high-frequency region (Figures S4ii–S4iv). While in the low-frequency region, the shift was smaller, ~5–10 dB (Figure S4i). These shifts of DPOAE thresholds recovered by 2 weeks after noise exposure. Other experimental

Please cite this article in press as: Mukherjee et al., Local magnetic delivery of adeno-associated virus AAV2(quad Y-F)-mediated BDNF gene therapy restores hearing after noise injury, Molecular Therapy (2021), https://doi.org/10.1016/j.ymthe.2021.07.013

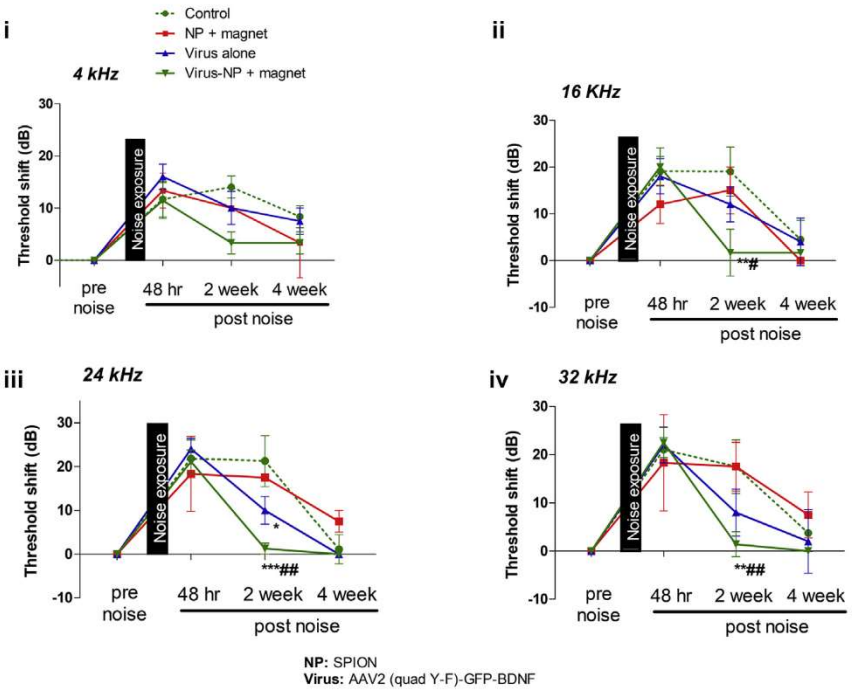

Figure 4. Magnetic targeting of AAV2(quad Y-F)-BDNF-SPION recovers the noise-induced ABR threshold shift faster

Representative traces of ABR before and after the noise exposure, evoked by pure tones at 4 kHz (i), 16 kHz (ii), 24 kHz (iii), and 32 kHz (iv). A 2-h exposure to an octave band (8–16 kHz) noise at 110 dB SPL produced an ~10-dB to ~25-dB shift of ABR threshold over the pre-noise threshold 48 h after the noise exposure. Threshold shifts were smaller in low frequency (i) and relatively higher in high frequencies (ii–iv). ABR threshold shifts recovered either partially or fully to normal pre-exposure values by 4 weeks after the noise exposure, in case of the control ears (green dotted line), and SPION-treated ears (NP + magnet, red line). ABR threshold shifts in the AAV2(quad Y-F)-BDNF-SPION magnetically targeted ears (virus-NP + magnet, green solid line) were recovered almost fully to pre-noise exposure value by 2 weeks after noise exposure (i–iv), whereas ABR threshold shifts were only partially recovered by 2 weeks and fully recovered by 4 weeks of noise exposure in AAV2(quad Y-F)-BDNF alone-treated ears (virus alone, blue line). Black vertical bars indicate the time of noise exposure. Graphs represent mean ± SEM values of the threshold shift. *$p < 0.05$, **$p < 0.01$, ***$p < 0.001$ (versus control); #$p < 0.05$, ##$p < 0.01$ (versus SPION + magnet); n = 5–12 animals.

groups followed a similar pattern without any significant differences. We found a trend of elevation in threshold or incomplete recovery at 4 weeks in the 16- and 32-kHz regions in control, SPION alone with magnetic targeting, and AAV2(quad Y-F)-BDNF-alone (without magnet) groups. However, there was complete recovery at all frequencies observed in the AAV2(quad Y-F)-BDNF-SPION with magnetic targeting group, although there were no statistically significant differences (Figures S4i–S4iv; $p > 0.18$).

With the moderate and significant recoveries in ABR thresholds after 2 weeks of noise exposure and gene-therapy treatment, we proceeded to examine the suprathreshold neural response at low and high frequencies. ABR wave I amplitude and DP amplitude were calculated. A multilevel model was used to evaluate how the wave I amplitude changed as a function of the group, time point of testing, frequency, and level, as well as their interactions. The highest significant interaction terms indicated a marginally significant group by time by level interaction ($F(15,1537.76) = 1.548$, $p = 0.081$) and a significant group by frequency by level interaction ($F(15,1537.76) = 2.66$, $p = 0.0005$). The four-way interaction was not significant, in sum, suggesting that group differences as the ABR elicitor level increased depended mostly on frequency.

Figure 5i shows that in control ears, at low frequency (4 kHz) where changes in the ABR threshold were less, the ABR wave I amplitude did not change significantly (Figure 5i; $p > 0.16$) with the exception of a difference at 4 weeks post-noise exposure at 90 dB SPL ($p = 0.002$). However, in the 16-, 24-, and 32-kHz regions where the ABR threshold shifts were significantly higher (Figure 4), ABR wave I amplitudes of the control group were significantly attenuated (Figures 5ii–5iv). Wave I amplitudes at these high-frequency regions were reduced by ~40%–50% after 48 h of noise exposure (mainly at suprathreshold levels of 70–90 dB) and did not recover by 2 or 4 weeks post-noise exposure. To analyze the control group further in terms of gender differences, we checked if there is any difference in ABR wave I amplitude reduction after noise exposure between male and female rats. We did not find any significant difference in ABR wave I amplitude reduction after noise exposure between male and female rats (Figure S5). However, we found a trend of lower ABR wave I amplitude in female rats at 16 kHz (and 32 kHz frequency in pre-noise condition), mainly at a higher noise level (Figure S5ii). But these changes were not statistically significant. As in our experimental setup, we did not find any significant different effects of noise exposure on the ABR wave I amplitude between male and female rats; we combined the male and female rat data to analyze the impact of magnetic targeting of AAV2(quad Y-F)-BDNF-SPION on noise-induced ABR wave I amplitude reduction. In the AAV2(quad Y-F)-BDNF-SPION with the magnetic targeting group, this attenuation of ABR wave I amplitude was only temporary, at 48 h. The magnetically targeted AAV2(quad Y-F)-BDNF-SPION group quickly recovered ABR amplitude by ~80%–90% in the 16-kHz region, ~80% in the 24-kHz region, and ~70%–80% in the 32-kHz region by 2 weeks of noise exposure. Post hoc tests from the multilevel model support these observations, showing a reduced ABR wave I amplitude in the control group compared to the AAV2(quad Y-F)-BDNF-SPION with the magnetic targeting group at 80 and 90 dB SPL from 2 to 4 weeks at 16 kHz and above ($p < 0.019$). Differences were also found at 70 dB SPL at 16 and 32 kHz at both 2 and 4 weeks post-noise exposure ($p < 0.045$) and for the 60-dB SPL condition (24 kHz at 2 weeks, $p = 0.033$, and 32 kHz at 4 weeks, $p = 0.040$). This suggests that

Please cite this article in press as: Mukherjee et al., Local magnetic delivery of adeno-associated virus AAV2(quad Y-F)-mediated BDNF gene therapy restores hearing after noise injury, Molecular Therapy (2021), https://doi.org/10.1016/j.ymthe.2021.07.013

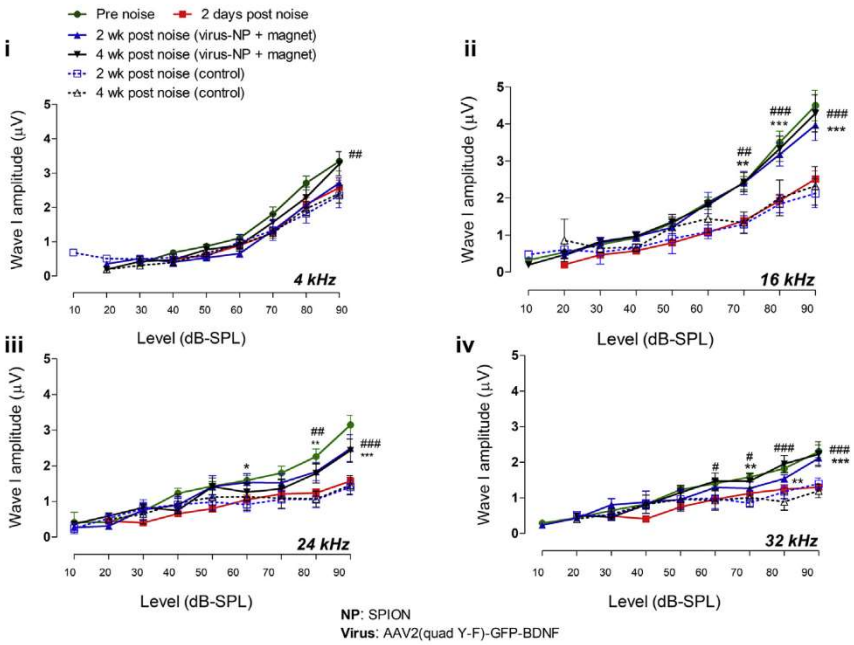

Figure 5. Wave I amplitudes at high frequencies were permanently attenuated

Representative traces of ABR wave I amplitude evoked by suprathreshold tones at 4 kHz (i), 16 kHz (ii), 24 kHz (iii), and 32 kHz (iv) frequencies. 2 days following the noise exposure, the suprathreshold amplitude of ABR wave I (red line), which is related to the far-field response of the cochlear nerve, was permanently reduced from their pre-exposure values at 16 kHz, 24 kHz, and 32 kHz in control ears (red line, black dotted line, and blue dotted line). Magnetic targeting of AAV2(quad Y-F)-BDNF-SPION (virus-NP + magnet) in the inner ear significantly recovers ABR wave I amplitude by 2 weeks of the noise exposure (blue solid line) and maintains in the recovered stage even after 4 weeks of the noise exposure (black solid line). Graphs represent mean ± SEM values of the threshold shift. *p < 0.05, **p < 0.01, ***p < 0.001 (2 weeks post-noise control versus 2 weeks post-noise virus-NP + magnet); #p < 0.05, ##p < 0.01, ###p < 0.001 (4 weeks post-noise control versus 4 weeks post-noise virus-NP + magnet); n = 12 (control) and 11 (AAV2(quad Y-F)-BDNF-SPION with magnetic targeting) animals.

recovery remains stable at 4 weeks post-noise exposure and gene therapy treatment. We did not observe such recovery of wave I amplitude in the AAV2(quad Y-F)-BDNF-alone (without magnet) group after finding a comparable three-way interaction among group, frequency, and level comparing AAV2(quad Y-F)-BDNF groups with and without magnetic targeting ($F(15,965.55) = 2.587$, $p = 0.0008$) (Figure S6).

For changes in DPOAEs, multilevel modeling indicated a group by frequency interaction ($F(3,734.83) = 7.61$, p & lt; 0.001). Post hoc comparisons, however, indicated that the differences between groups were mainly due to spurious variation in animals before AAV2(quad Y-F)-BDNF with magnetic targeting was applied, with differences in pre-and post-noise measurements at 16 and 24 kHz from 50 to 80 dB (p & lt; 0.04). No differences were found after AAV2(quad Y-F)-BDNF with magnetic targeting (Figure S7), with the exception of a minor difference at the 2-week measurement, evoked at 16 kHz at 60 dB ($p = 0.43$), which was not sustained at 4 weeks ($p = 0.18$). These results suggested the loss of neuronal function due to noise exposure recovered after magnetic targeting of BDNF gene therapy in high-frequency regions without any widely significant changes in OHCs.

Next, together with minimal changes in the DPOAE threshold previously reported and to confirm that noise exposure did not have a significant effect on hair cells, we labeled hair cells with anti-myosin VII A antibody. The results did not show notable changes in OHCs and IHCs morphology and count in any of the experimental groups at any post-noise exposure time points. Figure S8 shows normal arrays of OHCs and IHCs throughout the cochlea of naive control (Figures S8a–S8c), noise control (Figures S8d–S8f), and AAV2(quad Y-F)-BDNF-SPION with magnetic targeting groups (Figures S8g–S8i) at 4 weeks after noise exposure. This normal morphology of OHCs and IHCs confirmed the minimal changes in the DPOAE threshold and amplitudes assessed previously. However, with the recovery of ABR threshold and amplitude after BDNF treatment, we examined the effect of noise exposure on the synapses between IHCs and SGNs. Synapses between IHCs and SGNs were visualized by immunostaining presynaptic ribbon protein, the C-terminal-binding protein 2 (CtBP2), and postsynaptic protein, glutamate receptor subunit 2 (GluA2). Presynaptic ribbon protein and postsynaptic protein pair (CtBP2/GluA2 pair) were counted in all three regions (apex, <8 kHz; mid-turn, 8–20 kHz; and basal turn, >20 kHz) of the cochlea. We found an average of ~10–13 CtBP2/GluA2 pairs per IHC in the naive control group (Figure 6). Anti-CtBP2 also stains IHC nuclei, which showed an intact array of IHCs throughout the cochlear turns after noise exposure in all of the experimental groups (Figure 6). Although the IHCs were intact, there was an observable degeneration of presynaptic ribbon protein and postsynaptic protein counts after noise exposure in the control group at 4 weeks (Figure 6ii). This degeneration was found mainly in the high-frequency regions (basal and mid-turn, >8 kHz frequency region) (Figures 6ii, 6ii e, and 6ii f), which were associated with a previous threshold shift and permanent attenuation of ABR wave I amplitude seen in the high-frequency regions (16–32 kHz) (Figures 4 and 5). The results demonstrated ~60% reduction of presynaptic ribbon protein/postsynaptic protein pair counts in the basal turn region and ~65% reduction in the mid-turn region by 4 weeks after noise exposure (Figure 6iii). In contrast, presynaptic/postsynaptic pair counts in the low-frequency apex region appeared to be less affected after noise exposure (Figure 6iii; ~25% reduction). Similar effects were observed in the SPION-alone group (data not

Please cite this article in press as: Mukherjee et al., Local magnetic delivery of adeno-associated virus AAV2(quad Y-F)-mediated BDNF gene therapy restores hearing after noise injury, Molecular Therapy (2021), https://doi.org/10.1016/j.ymthe.2021.07.013

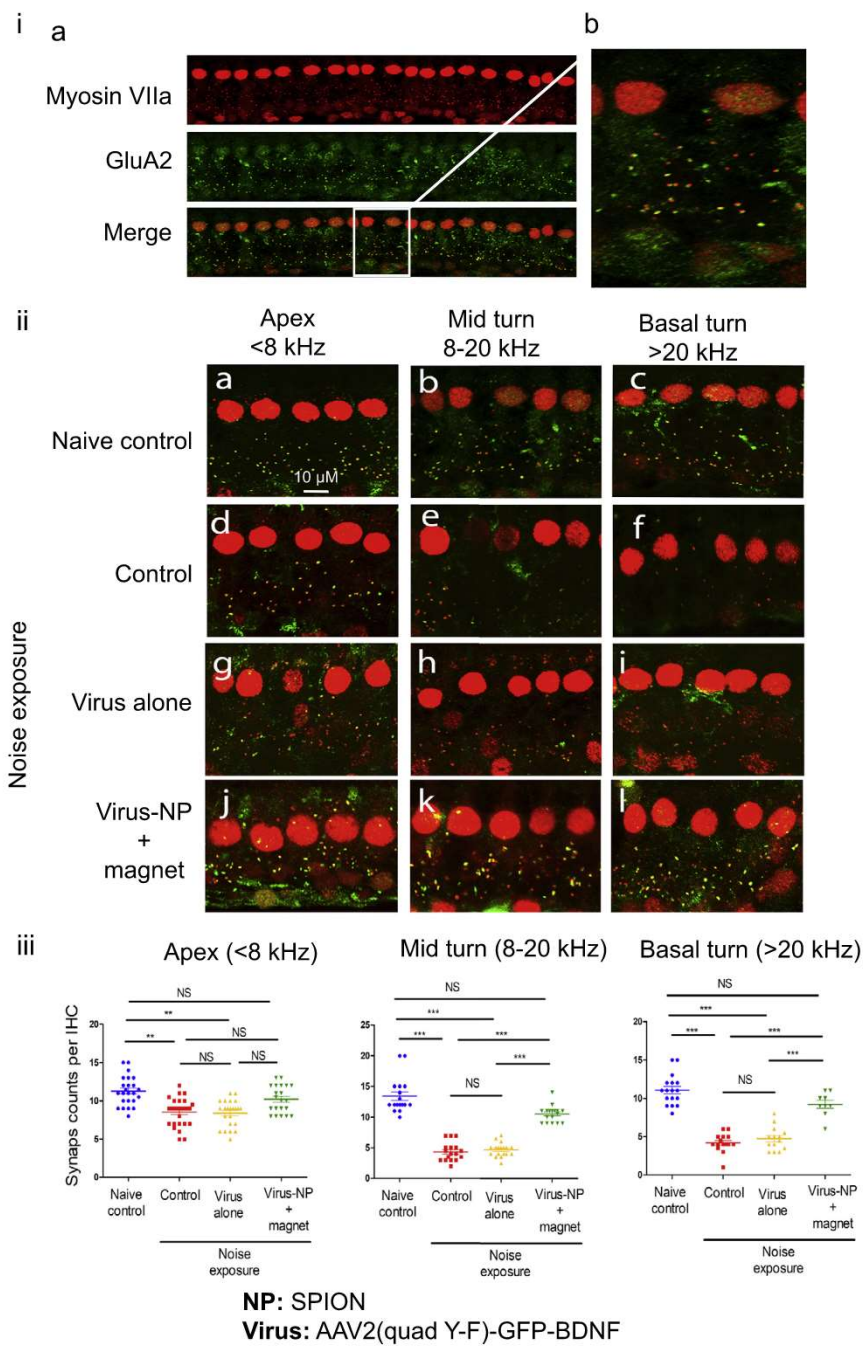

Figure 6. Despite threshold shift recovery and intact hair cells, noise exposure induced loss of cochlear synaptic terminals

Representative confocal z stack images of IHC synaptic immunopuncta of naive control (i, a and b; ii, a–c), noise control (ii, d–f), virus alone-treated (ii, g–i) and virus-NP with magnetic targeting-treated (ii, j–l) rats. (i, a) Presynaptic ribbon proteins were stained with anti-CtBP2 (red channel); postsynaptic proteins were stained with GluA2 (green channel). (i, b) Magnified inset shows juxtaposition in the x to y plane. (ii) Immunostaining confocal images (merge) show presynaptic and postsynaptic protein pairs (CtBP2/GluA2 pair) in the IHC area of untreated (naive) control ears (ii, a–c), noise control ears (ii, d–f), AAV2(quad Y-F)-BDNF alone-treated ears (virus alone; ii, g–i), and AAV2(quad Y-F)-BDNF-SPION with magnetic targeting ears (virus-NP + magnet; ii, j–l). Anti-CtBP2 also stains the nucleus of IHCs. Immunostaining for the noise-exposed group ears (ii, d–l) was done 4 weeks after the noise exposure. IF data shown are representative of at least 4 independent experiments using different rats. Photomicrographs were all taken in the same setting (60× zoom) and exposure time. The scattered plots (iii) show the average synapse counts (CtBP2/GluA2 pair) per IHC in the cochlea apex region, mid-turn, and basal turn. The average number of synapses is reduced after noise exposure in apex, basal turn, and mid-turn. AAV2(quad Y-F)-BDNF alone treatment did not have any effect on the reduction of synapses number per hair cell (ii, g–i, and iii). Magnetic targeting of AAV2(quad Y-F)-BDNF-SPION recovers the loss of synapses throughout the cochlear turns by 4 weeks post-noise exposure (ii, j–l, and iii). Scatter-plots indicate mean ± SEM values of ribbon per IHC. $^{**}p < 0.01$, $^{***}p < 0.001$; n = 4 animals (multiple sections were counted from each cochlear turn) in each group.

shown) and AAV2(quad Y-F)-BDNF-alone (without magnet) group (Figures 6ii, 6ii g–6ii i). However, magnetically targeted AAV2(quad Y-F)-BDNF-SPION showed complete recovery of presynaptic ribbons and postsynaptic proteins by 4 weeks after noise exposure (Figures 6ii, 6ii jJ–6ii l).

These observed differences were statistically confirmed using a Poisson regression model, finding a significant interaction term between the group and cochlear location ($\chi^2(1) = 51.73$ $p < 0.001$). Post hoc comparisons suggested that the control group had higher synaptic counts than the noise control group and AAV2(quad Y-F)-BDNF-only group at the base, mid-turn region, and apex ($p < 0.05$) and was not different from the AAV2(quad Y-F)-BDNF-SPION with magnetic targeting group at any location ($p > 0.064$). In contrast, the AAV2(quad Y-F)-BDNF-SPION with magnetic targeting group had higher synaptic counts than the virus-only and noise control groups at the base and mid-turn region ($p < 0.05$) but not the apex ($p > 0.18$). No other comparisons were significantly different.

BDNF is known to play a crucial role in the development and maintenance of synaptic ribbons in the inner ear.[10,12,13] To examine the neuroprotective role of the BDNF gene over the entire time course of gene therapy treatment, we quantified the expression level of BDNF mRNA in the noise-exposed rat cochlea before and after local

Please cite this article in press as: Mukherjee et al., Local magnetic delivery of adeno-associated virus AAV2(quad Y-F)-mediated BDNF gene therapy restores hearing after noise injury, Molecular Therapy (2021), https://doi.org/10.1016/j.ymthe.2021.07.013

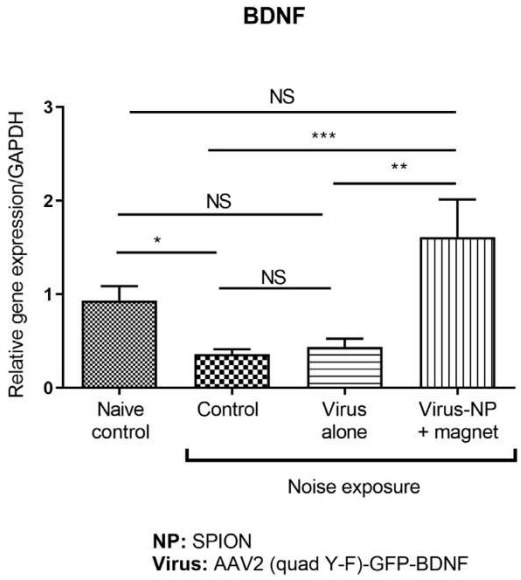

Figure 7. Local magnetic delivery of AAV-BDNF recovers the reduction in BDNF mRNA level after noise injury

Relative gene expression of the BDNF gene in the cochlea of control, AAV2(quad Y-F)-BDNF alone (virus alone), and AAV2(quad Y-F)-BDNF-SPION with magnetic targeting (virus-NP + magnet) treated animal before and after noise exposure. The expression level of BDNF mRNA in rat cochlea was significantly reduced after 2-h exposure to an octave band (8–16 kHz) noise at 110 dB SPL. Corrected post hoc results showed that BDNF expression was reduced by more than 2.5-fold after noise exposure in naive control ($p = 0.052$; $p = 0.039$ uncorrected). The AAV2(quad Y-F)-BDNF-alone group did not show any significant recovery of the BDNF mRNA level. But magnetic targeting of AAV2(quad Y-F)-BDNF-SPION not only recovers the BDNF mRNA level but surpasses the baseline level (naive control ear). Rat cochleae were collected 4 weeks after delivering AAV2(quad Y-F)-BDNF ± SPION and processed for RT-PCR. Bar diagrams indicate mean ± SEM values of relative gene expression. *$p < 0.05$, **$p < 0.01$, ***$p < 0.001$; $n = 8$ (naive control group), 5 (noise control group), (AAV2(quad Y-F)-BDNF alone group), and 5 (AAV2(quad Y-F)-BDNF with magnetic targeting) animals.

delivery of AAV2(quad Y-F)-BDNF (Figure 7). A one-way ANOVA indicated that BDNF expression after noise exposure was different between groups ($F(3,18) = 5.90$, $p = 0.005$). Corrected post hoc results showed that BDNF expression was reduced by more than 2.5-fold after noise exposure in naive control ($p = 0.052$; $p = 0.039$ uncorrected). AAV2(quad Y-F)-BDNF alone (without magnet) did not show any recovery or improved expression of the BDNF mRNA level. However, magnetic targeting of AAV2(quad Y-F)-BDNF-SPION not only recovered the reduction in gene expression (BDNF expression larger than the noise-exposed control, $p = 0.005$) but also descriptively surpassed the baseline value of the BDNF gene-expression level of naive control rat by 2-fold (this effect was not statistically significant, $p = 0.115$; Figure 7). The BDNF gene expression appeared stable at 4 weeks post-treatment (Figure 7) and comparable to the initial level post-transduction (Figure 3ii).

DISCUSSION

An efficient and effective drug-delivery technique to the cochlea is not yet established and thus creates a major barrier toward the treatment of inner-ear disorders. Systemic administration techniques are not effective because of the blood-labyrinth barrier.

On the other hand, local delivery techniques are challenging because of the complexity of the inner ear. In the intratympanic administration approach, drugs are deposited in the round window niche and allowed to diffuse into the inner ear through the RWM. This approach requires the ability of the drug to diffuse through the RWM to scala tympani based on size, polarity, and duration of contact with RWM.[14,15] Hence, the majority of the drug gets lost by clearance through the eustachian tube.[28] Additionally, this approach does not guarantee the effective distribution of the drug along the cochlea due to the low flow rate of perilymph within the cochlea.[29] To overcome this nonuniformity of drug distribution along the cochlea, different intracochlear administration techniques have been proposed, including direct round window injection, cochleostomy, and canalostomy. These intracochlear techniques are invasive with the risk of further hearing and balance loss and infection.[15] To address this problem, it is necessary to develop a minimally invasive approach to delivering drugs while achieving a high concentration of drug delivery and better distribution within the cochlea. Drug-loaded nanoparticles take advantage of magnetic targeting delivery to the inner ear.[29]

SPIONs are the ideal candidate for delivering drug substances because of their excellent biocompatibility and superparamagnetism. Paramagnetic properties of SPIONs enable their use as MR contrast agents, and they can also be targeted to specific organs, for cancer treatment, and for imaging.[30,31] In our study, we used SPIONs as a vehicle to carry AAV to the inner ear. The effective and efficient delivery was captured as a decreased signal on MRI (Figure 1). The distribution of SPIONs via magnetic targeting was recorded throughout the cochlea at different turns as well as the vestibule and semicircular canal (Figure 1). More importantly, we did not observe any significant loss of hearing and hair cells in a non-deafened ear following the magnetic delivery of SPIONs (Figure 2). SPIONS are generally very safe *in vivo* and can be cleared by uptake into phagocytic cells and the reticuloendothelial system, where they degrade within 4–6 weeks and are recycled in the normal iron pool.[13,32,33] The minimally invasive nature of local magnetic targeting can potentially be applied in a clinical setting. After an intratympanic injection, instead of relying on passive diffusion of the drug through the RWM, SPIONs carrying drugs can be delivered actively and directly through the RWM via an external magnetic force. Improved delivery and distribution of drugs into the cochlea, and potentially vestibular system, are particularly useful for the implementation of treatment or prevention of different inner-ear conditions, including NIHL, tinnitus, and Meniere's disease.

AAV is an ideal gene-delivery vector because of its low immunogenicity and persistent gene expression in non-dividing cells. As the cochlea is isolated from surrounding tissues, it is an ideal organ for local viral gene therapy without potential systemic effects. Studies have also shown that different AAV serotypes can mediate gene expression and

allow recovery of auditory function partially in mouse models of hereditary hearing loss and NIHL.[34] One potential drawback with AAV-mediated gene therapy was that conventional AAVs infect inner-ear hair cells and neurons with low efficiency.[35] To overcome this problem, several modifications have been made to create recombinant AAVs. Anc80L65, AAV2.7m8, AAV-ie, and AAV9-PHP.B have been shown to infect cochlear IHCs and OHCs with high efficiency and drive the expression of desired genes in the inner ear.[34,36–38] Phosphorylation of tyrosine residue in the AAV capsid serves as a signal for AAV vector ubiquitination and degradation.[39] Hence, the substitution of tyrosine residue with phenylalanine residue reduces virus degradation and enhances gene expression.[40–43] In our study, recombinant AAV2 with quad mutations of Y-F (Y730F, Y500F, Y444F, and Y272F) was used for the first time to facilitate gene therapy in the rat inner ear. Our results showed successful and highly efficient transfection of cochlear IHCs and OHCs (Figure 3i) and overexpression of GFP and BDNF mRNA following magnetic targeting of AAV2(quad Y-F)-GFP-BDNF-SPION treatment (Figures 3iv and 7). Cochleae of the rats that were treated with AAV2(quad Y-F)-GFP-BDNF alone (without magnet) did not show any significant overexpression of GFP and BDNF mRNAs. Presumably, there was not enough AAV2(quad Y-F) passive diffusion across the RWM to significantly enhance gene expression. These results demonstrate the critical utility of magnetic targeting in the delivery of viral gene therapy to improve local delivery into the inner ear.

Proper hearing relies on the synaptic transmission at the ribbon synapse between cochlear IHCs and peripheral nerve fibers of SGNs. Synaptic ribbons are the structural hallmark of IHC afferent synapse and are involved in holding synaptic vesicles to the active zone.[44,45] Ribbon-less synapses result in smaller wave I peak amplitudes without any difference in DPOAE threshold in the knockout (KO) mouse.[45] In this study, we found long-term or permanent loss of the ABR wave I amplitudes (~50%) and presynaptic ribbon protein/postsynaptic proteins pairs (~60%–65%) (Figures 5 and 6) in the control ear, despite the recovery of hearing thresholds (Figures 4 and S3 and S4). Previous studies have also shown that sound-evoked neural potential thresholds are insensitive to diffuse neuronal loss if the OHCs function normally.[16,46] Loss of synapses is reflected in the suprathreshold ABR wave I amplitude because ABR amplitude depends on the sound-evoked discharge probability of each responding fiber and the number of the neuronal fibers that are responding synchronously.[1,47] Thus, a loss of ~60%–65% of the synapses in the basal turn and mid-turn (Figure 6) of control ears resulted in ~50% loss of the suprathreshold ABR wave I amplitude at 16 kHz, 24 kHz, and 32 kHz (Figure 5) without significant change in ABR threshold of the control group. Treatment using magnetic targeting of AAV2(quad Y-F)-BDNF-SPION prevented this loss of synapses and allowed recovery of suprathreshold ABR wave I amplitude in these anatomical regions. DPOAE and ABR thresholds are sensitive to hair cell damage but insensitive to neuronal damage while hair cells are intact. Hence, dependency on ABR and DPOAE threshold to screen for NIHL in the clinical setting might not be an appropriate approach.

Synaptic connections between SGNs and hair cells are vulnerable to damage from noise exposure.[5] Recent studies have shown that noise exposure can damage SGN peripheral fibers and the synapse rapidly due to the release of glutamate from the presynaptic ribbons.[48,49] BDNF is known to be critical for establishing synapses during development and maintaining hearing.[7–13] Studies have shown that overexpression of BDNF can preserve SGN in deaf ears.[50–52] Additionally, BDNF has been shown to enhance the formation of new presynaptic and postsynaptic ribbons in rat cochlea explants, prevention of reduction of SGN fiber, and synaptic ribbons in an *ex vivo* noise-damage model.[53] Another study has shown that BDNF is crucial for the maintenance of ribbon numbers in high-frequency cochlear turns in mice.[54] BDNF can also prevent ABR threshold shift changes caused by ototoxicity.[55] In this study, stable overexpression of BDNF was achieved with magnetic delivery of AAV2(quad Y-F)-BDNF-SPION in the inner ear (Figures 3 and 7). We also found that noise injury significantly reduced the mRNA level of the BDNF gene below the baseline level (Figure 7). Local magnetic delivery of AAV2(quad Y-F)-BDNF-SPION not only recovered this reduction of BDNF mRNA level but also surpassed the native level by 2-fold (Figure 7). The stable overexpression of BDNF influenced the faster recovery of ABR threshold reduction by 2 weeks, complete recovery of suprathreshold ABR wave I amplitude, and synaptic ribbon count by 4 weeks. The normal development and maintenance of SGN are regulated by neurotrophic factors produced by hair cells and supporting cells of the organ of Corti. In this study, we did not examine the viral transduction, transgene expression, morphology, and number of SGNs with respect to viral gene therapy and noise exposure. However, with the recovery of ABR wave I amplitude and synaptic count, an assumption has been made that SGNs are likely not affected in this experimental paradigm. Future research on the long-term maintenance of SGNs and auditory nerve fibers (weeks to months post-treatment) should be considered.

The data we report, showing the effectiveness and efficiency of the local magnetic targeting delivery of gene therapy to the inner ear, support other recent advances in restoring structure and function in the NIHL model. The findings provide milestones in progress toward a local drug-delivery technique that is minimally invasive, safe, and repeatable to treat NIHL or other inner-ear diseases. In addition, we provide a proof of principle that NIHL is amenable to treatment and prevention aimed at enhancing synaptic survival, thereby providing an avenue for recombinant gene therapy. The improvement of long-term neurotrophic support in the inner ear will augment the outcome of future regenerative therapies to treat inner-ear diseases.

Although this study has several strengths, it has some limitations. The main caveat for interpreting our study is that we combined the six male and six female animals in our analysis in order to increase statistical power, but there are too few independent observations in each sex to properly power a separate comparison of male and female rats on the effect of noise exposure and the role of the magnetic delivery of AAV2(quad Y-F)-BDNF-SPION in the prevention of NIHL. Male and female rat comparison results (Figures S1, S3, and S5) should

Please cite this article in press as: Mukherjee et al., Local magnetic delivery of adeno-associated virus AAV2(quad Y-F)-mediated BDNF gene therapy restores hearing after noise injury, Molecular Therapy (2021), https://doi.org/10.1016/j.ymthe.2021.07.013

Table 1. Animal groups and experimental schedule for our study of SPION-mediated local magnetic delivery of BDNF gene therapy into the inner ear to prevent NIHL

Group A no noise exposure						Group B noise exposure			
		Treated ear (left ear)					Treated ear (left ear)		
Day	naive control (right ear)	(1) SPION without magnet	(2) SPION with magnet	(3) AAV2(quad Y-F) without magnet	(4) AAV2(quad Y-F)-SPION with magnet	noise control (right ear)	(1) SPION with magnet	(2) AAV2(quad Y-F) without magnet	(3) AAV2(quad Y-F)-SPION with magnet
		← Pre-treatment hearing test →							
0		local delivery of SPION and MRI	local delivery of SPION, magnetic targeting, and MRI	local delivery of AAV2 (quad Y-F)	local delivery of AAV2(quad Y-F)-SPION and magnetic targeting	← noise exposure 110 dB for 2 h →			
2						← 48 h post-noise hearing test →			
3						local delivery of SPION and magnetic targeting	local delivery of AAV2(quad Y-F)	local delivery of AAV2(quad Y-F)-SPION and magnetic targeting	
14	← 2-week post-treatment/surgery hearing test and sample collection →								
28	← 4-week post-treatment/surgery hearing test and sample collection →								

be interpreted cautiously due to the small sample size. It is important to evaluate effects separately for each sex because the difference in estrous cycle hormonal profile in male and female rats can generate different response levels to noise trauma. Also, the treatments for NIHL may appear effective for a mix of sexes but may not be effective for each sex separately.[56] We encourage adequate sample sizes in future studies to examine the effect of noise exposure and BDNF gene therapy in different biological sexes.

MATERIALS AND METHODS

Animal

All animal care and handling were approved by the Canadian Council on Animal Care and the Sunnybrook Animal Care Committee Regulations and were performed using accepted veterinary standards. Wild-type Long-Evans rats were obtained from Charles River Laboratories (Canada). Equal numbers of male and female rats were used, and the rats were 6–8 weeks old at the onset of the experiments. All rats were housed under standard conditions: 12:12 light/dark cycle and controlled room temperature (22°C ± 1°C) and were fed regular rat chow *ad libitum* with free access to water throughout the experimental procedure. After brief acclimatization to our vivarium, the cochlear function was tested by measurement of ABRs and DPOAEs. Animals were then randomly assigned to one of the two main groups: no noise exposure group (group A) and noise exposure group (group B). Group A animals were randomly divided into 4 groups: (1) SPION alone without magnet group, (2) SPION with magnet group, (3) AAV2(quad Y-F)-alone group (without magnet), and (4) AAV2(quad Y-F)-SPION with magnetic targeting groups. Right ears were used as naive control group ears. Group B animals were randomly divided into 3 groups: (1) SPION alone with magnet group, (2) AAV2(quad Y-F)-alone group (without magnet), and (3) AAV2(quad Y-F)-SPION with magnetic targeting groups. The right ears of group B animals were used as noise control ears. The overall animal grouping and study design are shown in Table 1.

Acoustic overexposures

NIHL in rats was achieved following the protocol explained by Kujawa and Liberman.[1] Briefly, the rats were anesthetized by intraperitoneal (i.p.) injection of ketamine (100 mg/kg) and xylazine (20 mg/kg) and placed in a small cage. The cage, with 1–2 rats, was placed directly below the horn of the sound-delivery loudspeaker in a small reverberant chamber. The acoustic overexposure stimulus was an octave band of noise (8–16 kHz) at 110 dB SPL, for 2 h. The noise level was calibrated to ensure 110 dB SPL delivery immediately for each exposure session.

Cochlear function testing

ABRs and DPOAEs were recorded using the Tucker-Davis Technologies (TDT) system 3 RZ6 in a closed field with individual ears tested separately as described by Kujawa and Liberman.[1] The animals were anesthetized with an i.p. injection of ketamine (100 mg/kg) and xylazine (20 mg/kg). Acoustic stimuli were delivered through the TDT acoustic system speakers connected to the ear canal.

ABR stimuli—5 ms, single-channel, cosine-squared, gated tones—were delivered 21 times/s at frequencies of 4 kHz, 8 kHz,16 kHz, 24 kHz, and 32 kHz. The sound level was incremented in 10 dB steps ranging from 10 dB to 100 dB. ABR threshold was defined as the lowest sound level at which a reproducible waveform was identified following a visual inspection. To calculate wave I amplitude, the averaged ABR waveforms were imported into MATLAB (R2018a; MathWorks, Natick, MA, USA). With the use of custom-processing scripts, wave I amplitude was defined as the

difference between the positive and negative deflections of wave I (P1 and N1, respectively). DPOAEs were recorded using two simultaneous continuous pure tones (frequencies 1 and 2 [f1 and f2]), differing by 20%. Sound levels were swept in 10 dB steps from 20 to 80 dB. The DP 2f1−f2 was measured in response to f1 and f2. DPOAEs were measured at the center frequencies (fcs) from 4 kHz to 32 kHz. DPOAE amplitude (decibel SPL) was calculated to measure the changes in the DPOAE amplitude. DPOAE threshold was determined visually as the lowest noise level to observe a DP over background noise.

Nanoparticle and AAV vector

A recombinant AAV2 vector was obtained from Ocular Gene Therapy Core at the University of Florida. This recombinant vector includes an AAV2 vector with four surface-exposed capsid tyrosine residue replaced by phenylalanine (Y730F, Y500F, Y444F, and Y272F), expressing a green fluorescent protein reporter gene under the control of a chicken β actin (CBA) promoter. The vector was packaged with a rat BDNF transgene coding sequence with an internal ribosome entry site (IRES).

Mag4C-Ad SPIONs (OZ Biosciences, San Diego, CA, USA) were used to capture AAV2(quad Y-F) through electrostatic and hydrophobic interaction as per the manufacturer's protocol. In brief, 6 μL of AAV2(quad Y-F) was mixed with 20 μL of SPIONs and was incubated at room temperature for 30 min before round window administration and magnetic targeting delivery.

Round window administration of BDNF and magnetic targeting delivery

3 days after the noise exposure, animals underwent general anesthesia using 2%–3% isoflurane for the surgical intervention. Round window administration was done via a postauricular approach under sterile conditions and using a surgical microscope. A 10-mm postauricular skin incision was made, and subcutaneous tissues and superficial fascia of the neck were bluntly dissected. After exposing the otic bulla, tympanotomy was performed using a 1-mm diamond burr until the RWM was visible. 26 μL solution of SPIONs alone, AAV2(quad Y-F)-BDNF-GFP alone (6 μL virus + 20 μL saline), or AAV2(quad Y-F)-BDNF-GFP-SPION (6 μL virus + 20 μL SPION) was deposited onto the RWM using a Hamilton syringe. The tympanotomy hole was sealed with muscle and fascia, and the surgical wound was closed with 4-0 Vicryl sutures (Ethicon) and Vetbond (3M). The right ears were untreated and used as same-animal controls. A 1.0-Tesla magnet (5 × 5 × 5 cm; K&J Magnetics, Pipersville, PA, USA) was placed on the contralateral ear, near the right eye, for 30 min after surgery, for groups A2, A4, B1, and B3.

MRI

The rats' ears were scanned immediately following the treatment using a 7T Horizontal Bore Advance BioSpec 70/30 scanner (Bruker BioSpin, Ettlingen, Germany) with an 8-cm inner-diameter volume transmit coil and a 20-mm loop receiver coil placed immediately over the ears of the animal. Animals were maintained under anesthesia using 1.5%–2% isoflurane.

Imaging was performed using a 3D Rapid Imaging with Refocused Echo (RARE) sequence, with repetition time (TR) 1,800 ms, echo train of 40, and spacing of 7.2 ms for an effective echo time of 100.8 ms, 32 × 32 × 6.4 mm^3 field of view, with an isotropic resolution of 0.1 mm^3 and total imaging time of 1 h and 7 min.

This sequence was specially optimized to visualize the fluid-filled structures of the inner ear bilaterally, whereas the 3D isotropic resolution allowed image reconstruction in all 3 planes in addition to 3D rendering of the inner ear. The presence of SPIONs causes a signal loss (black signal) in these images. The degree of signal loss was quantified in MATLAB (MathWorks, Natick, MA, USA) by normalization using the signal intensity from the corresponding region of the contralateral ear for a set of 5 ROIs from the apex, mid-turn, basal turn, and utricle. 3D renderings were done using the ImageJ 3D Viewer plug-in.[57]

RNA isolation and RT-PCR

At the end of the experimental period, rats were sacrificed via cervical dislocation. Cochleae were collected and stored in liquid nitrogen. For RNA isolation, cochlea were crushed and homogenized in 1 mL TRIzol reagent (Invitrogen) using a QIAGEN hand-healed probe. Total RNA was isolated according to the manufacturer's instructions and was dissolved in diethylpyrocarbonate-treated water. Total RNA concentration and integrity were determined with a microgel bioanalyzer (Agilent Bioanalyzer 2100; Agilent, Mississauga, ON, Canada). RNA (1 μg) was treated with DNase and reverse transcribed using qScript cDNA SuperMix (Quanta Bioscience, Gaithersburg, MD, USA). The cDNA was amplified by quantitative real-time PCR using the TaqMan method with the ABI Prism 7500 PCR system (Applied Biosystems, Foster City, CA, USA) according to the manufacturer's protocol. RT-PCR probe and primer sets for BDNF, GFP, SOX2, and glyceraldehyde 3-phosphate dehydrogenase (GAPDH) in gene-expression assays were purchased from Applied Biosystems. Results were normalized to the expression of GAPDH. Relative gene expression was calculated using the comparative threshold (CT) method (Applied Biosystems).

Cochlear processing and immunohistochemistry

At the end of the experimental time point, rats were sacrificed and perfused, and cochleae were collected and fixed with 4% paraformaldehyde for 2 h at room temperature. Cochleae were then decalcified with Osteosoft (MilliporeSigma, Canada) solution at room temperature for 48 h and then micro-dissected into 3 pieces (basal turn, mid-turn, and apex) for whole-mount processing. After blocking the nonspecific sites with donkey serum albumin (5%, overnight [O/N]), cochlear pieces were incubated with primary antibody (1) CtBP2 (mouse anti-CtBP2 from BD Biosciences used, at 1:200), (2) anti-GluA2 antibody (mouse anti-GluA2 from Millipore, used at 1:500), (3) anti-myosin VII A (Proteus Bioscience, USA; used at 1:1,000), (4) anti-myosin VI (Santa Cruz Biotechnology, USA; used

at 1:1,000), and (5) GFP polyclonal Alexa Fluor 488 antibody (Thermo Fisher Scientific, Canada; used at 1:500) diluted in 1% donkey serum albumin overnight in a humidified chamber at 4°C. Appropriate secondary antibodies coupled to Alexa Fluor in the red channel and green channel were used at a dilution of 1:2,000. Alexa Fluor 488 phalloidin was obtained from Thermo Fisher Scientific (Canada) and was used at 1:500 dilution. Slides were mounted in ProLong Gold with 4′,6-diamidino-2-phenylindole (DAPI) (ProLong Gold Antifade Reagent with DAPI; Life Technologies). Pictures were taken with a Nikon confocal microscope. Oil-immersion objective of 60× digital zoom and 20× digital zoom were used. Images were captured with the same setting and exposure time for all pictures. Images were ported to image-processing software (Adobe Photoshop, ImageJ), where OHCs, IHCs, and synapses were manually counted and divided by the total number of IHC nuclei in the microscopic field (60−100 μM) and rounded to the nearest value to estimate synaptic count per IHC.

Statistical analysis

Statistics were calculated in R (R Core Team, 2019) using the afex and lme4 packages. All post hoc tests were conducted using the emmeans package and corrected for a false discovery rate using the Benjamini and Hochberg procedure.[58] For multilevel models (e.g., lmer), the maximum random effects structures that allowed for model convergence (and avoidance of singular fits) were included. Note that whereas this may keep type I error rates down,[59] maximization of the random effects structure can reduce statistical power.[60] Analysis of fixed effects in multilevel models was assessed using ANOVA, with degrees of freedom adjusted using Satterthwaite's method. Multilevel models were used to analyze ABR and DPOAE threshold shifts and ABR amplitude growth functions.

Synaptic count data were analyzed using a Poisson regression with predictors of group and cochlear location. The significance of the interaction term was calculated by comparing the Poisson model to a separate model where the interaction term was excluded and comparing the two models using a likelihood ratio test. Follow-up comparisons were computed in the *emmeans* package in R.

SPION MRI contrasts in Figure 1 were assessed using a 2 × 5 mixed effects ANOVA, and sphericity corrections were applied to degrees of freedom using the Greenhouse-Geisser method. In Figure 3, GFP expression was analyzed using a one-way ANOVA. For BDNF expression, Levene's test indicated a difference in variance between groups, and thus a Kruskal-Wallis test was conducted. Post hoc comparisons were computed using Wilcoxon rank sum tests and adjusted for false discovery rate. For Figure 7, BDNF expression was analyzed using a one-way ANOVA.

SUPPLEMENTAL INFORMATION

Supplemental information can be found online at https://doi.org/10.1016/j.ymthe.2021.07.013.

ACKNOWLEDGMENTS

The authors acknowledge the technical support from Dr. Benjamin Shapiro, Dr. Alain Dabdoub, and Mr. Moiz Charania and a grant from the Koerner Hearing Regenerative Foundation.

AUTHOR CONTRIBUTIONS

S.M. and T.N.L. conceived and designed research, prepared figures, and drafted the manuscript. S.M., W.O., M.K., and T.N.L. performed experiments. S.M., W.O., M.K., A.N., B.T.P., and T.N.L. analyzed data. S.M., W.O., B.T.P., and T.N.L. interpreted results of experiments. S.M., W.O., M.K., A.N., B.T.P., J.C., V.L., A.D., G.S., and T.N.L. edited and revised the manuscript and approved the final version of the manuscript.

REFERENCES

1. Kujawa, S.G., and Liberman, M.C. (2009). Adding insult to injury: cochlear nerve degeneration after "temporary" noise-induced hearing loss. J. Neurosci. *29*, 14077–14085.

2. Furman, A.C., Kujawa, S.G., and Liberman, M.C. (2013). Noise-induced cochlear neuropathy is selective for fibers with low spontaneous rates. J. Neurophysiol. *110*, 577–586.

3. Liberman, L.D., Suzuki, J., and Liberman, M.C. (2015). Dynamics of cochlear synaptopathy after acoustic overexposure. J. Assoc. Res. Otolaryngol. *16*, 205–219.

4. Liberman, M.C. (2015). Hidden Hearing Loss. Sci. Am. *313*, 48–53.

5. Kujawa, S.G., and Liberman, M.C. (2015). Synaptopathy in the noise-exposed and aging cochlea: Primary neural degeneration in acquired sensorineural hearing loss. Hear. Res. *330* (Pt B), 191–199.

6. Liu, H., Lu, J., Wang, Z., Song, L., Wang, X., Li, G.L., and Wu, H. (2019). Functional alteration of ribbon synapses in inner hair cells by noise exposure causing hidden hearing loss. Neurosci. Lett. *707*, 134268.

7. Shoji, F., Miller, A.L., Mitchell, A., Yamasoba, T., Altschuler, R.A., and Miller, J.M. (2000). Differential protective effects of neurotrophins in the attenuation of noise-induced hair cell loss. Hear. Res. *146*, 134–142.

8. Wan, G., Gómez-Casati, M.E., Gigliello, A.R., Liberman, M.C., and Corfas, G. (2014). Neurotrophin-3 regulates ribbon synapse density in the cochlea and induces synapse regeneration after acoustic trauma. eLife *3*.

9. Cunningham, L.L., and Tucci, D.L. (2015). Restoring synaptic connections in the inner ear after noise damage. N. Engl. J. Med. *372*, 181–182.

10. Sly, D.J., Campbell, L., Uschakov, A., Saief, S.T., Lam, M., and O'Leary, S.J. (2016). Applying Neurotrophins to the Round Window Rescues Auditory Function and Reduces Inner Hair Cell Synaptopathy After Noise-induced Hearing Loss. Otol. Neurotol. *37*, 1223–1230.

11. Wang, Y., Hirose, K., and Liberman, M.C. (2002). Dynamics of noise-induced cellular injury and repair in the mouse cochlea. J. Assoc. Res. Otolaryngol. *3*, 248–268.

12. Xu, Y.P., Shan, X.D., Liu, Y.Y., Pu, Y., Wang, C.Y., Tao, Q.L., Deng, Y., Cheng, Y., and Fan, J.P. (2016). Olfactory epithelium neural stem cell implantation restores noise-induced hearing loss in rats. Neurosci. Lett. *616*, 19–25.

13. Le, T.N., Straatman, L., Yanai, A., Rahmanian, R., Garnis, C., Häfeli, U.O., Poblete, T., Westerberg, B.D., and Gregory-Evans, K. (2017). Magnetic stem cell targeting to the inner ear. J. Magn. Magn. Mater. *443*, 385–396.

14. Nyberg, S., Abbott, N.J., Shi, X., Steyger, P.S., and Dabdoub, A. (2019). Delivery of therapeutics to the inner ear: The challenge of the blood-labyrinth barrier. Sci. Transl. Med. *11*, eaao0935.

15. El Kechai, N., Agnely, F., Mamelle, E., Nguyen, Y., Ferrary, E., and Bochot, A. (2015). Recent advances in local drug delivery to the inner ear. Int. J. Pharm. *494*, 83–101.

16. Dobson, J. (2006). Gene therapy progress and prospects: magnetic nanoparticle-based gene delivery. Gene Ther. *13*, 283–287.

17. Nishida, K., Tanaka, N., Nakanishi, K., Kamei, N., Hamasaki, T., Yanada, S., Mochizuki, Y., and Ochi, M. (2006). Magnetic targeting of bone marrow stromal cells into spinal cord: through cerebrospinal fluid. Neuroreport *17*, 1269–1272.

18. Wilhelm, C., Bal, L., Smirnov, P., Galy-Fauroux, I., Clément, O., Gazeau, F., and Emmerich, J. (2007). Magnetic control of vascular network formation with magnetically labeled endothelial progenitor cells. Biomaterials *28*, 3797–3806.

19. Loebinger, M.R., Kyrtatos, P.G., Turmaine, M., Price, A.N., Pankhurst, Q., Lythgoe, M.F., and Janes, S.M. (2009). Magnetic resonance imaging of mesenchymal stem cells homing to pulmonary metastases using biocompatible magnetic nanoparticles. Cancer Res. *69*, 8862–8867.

20. Pouponneau, P., Leroux, J.C., Soulez, G., Gaboury, L., and Martel, S. (2011). Co-encapsulation of magnetic nanoparticles and doxorubicin into biodegradable microcarriers for deep tissue targeting by vascular MRI navigation. Biomaterials *32*, 3481–3486.

21. Taylor, E.N., and Webster, T.J. (2011). Multifunctional magnetic nanoparticles for orthopedic and biofilm infections. Int. J. Nanotechnol. *8*, 21–35.

22. Kopke, R.D., Wassel, R.A., Mondalek, F., Grady, B., Chen, K., Liu, J., Gibson, D., and Dormer, K.J. (2006). Magnetic nanoparticles: inner ear targeted molecule delivery and middle ear implant. Audiol. Neurotol. *11*, 123–133.

23. Nacev, A., Komaee, A., Sarwar, A., Probst, R., Kim, S.H., Emmert-Buck, M., and Shapiro, B. (2012). Towards Control of Magnetic Fluids in Patients: Directing Therapeutic Nanoparticles to Disease Locations. IEEE Contr. Syst. Mag. *32*, 32–74.

24. Sensenig, R., Sapir, Y., MacDonald, C., Cohen, S., and Polyak, B. (2012). Magnetic nanoparticle-based approaches to locally target therapy and enhance tissue regeneration in vivo. Nanomedicine (Lond.) *7*, 1425–1442.

25. Depireux, D.A., Sarwar, A., Nacev, A., and Shapiro, B. (2014). Delivery of therapy to the inner ear via magnetic nanoparticles. 2014 Spring Symposium: From Lab to Life: Field Based Applications of MEMS & NEMS (MAMNA), pp. 1–4.

26. Ramaswamy, B., Roy, S., Apolo, A.B., Shapiro, B., and Depireux, D.A. (2017). Magnetic Nanoparticle Mediated Steroid Delivery Mitigates Cisplatin Induced Hearing Loss. Front. Cell. Neurosci. *11*, 268.

27. (2004−2013). Molecular Imaging and Contrast Agent Database (MICAD) [Internet]. (National Center for Biotechnology Information, National Institutes of Health), https://www.ncbi.nlm.nih.gov/books/NBK5330/.

28. Salt, A.N., and Plontke, S.K. (2005). Local inner-ear drug delivery and pharmacokinetics. Drug Discov. Today *10*, 1299–1306.

29. Lukashkin, A.N., Sadreev, I.I., Zakharova, N., Russell, I.J., and Yarin, Y.M. (2020). Local Drug Delivery to the Entire Cochlea without Breaching Its Boundaries. iScience *23*, 100945.

30. Dulińska-Litewka, J., Łazarczyk, A., Hałubiec, P., Szafrański, O., Karnas, K., and Karewicz, A. (2019). Superparamagnetic Iron Oxide Nanoparticles-Current and Prospective Medical Applications. Materials (Basel) *12*, E617.

31. Thomas, R., Park, I.K., and Jeong, Y.Y. (2013). Magnetic iron oxide nanoparticles for multimodal imaging and therapy of cancer. Int. J. Mol. Sci. *14*, 15910–15930.

32. Gupta, A.K., and Gupta, M. (2005). Cytotoxicity suppression and cellular uptake enhancement of surface modified magnetic nanoparticles. Biomaterials *26*, 1565–1573.

33. Weissleder, R., Stark, D.D., Engelstad, B.L., Bacon, B.R., Compton, C.C., White, D.L., Jacobs, P., and Lewis, J. (1989). Superparamagnetic iron oxide: pharmacokinetics and toxicity. AJR Am. J. Roentgenol. *152*, 167–173.

34. Isgrig, K., McDougald, D.S., Zhu, J., Wang, H.J., Bennett, J., and Chien, W.W. (2019). AAV2.7m8 is a powerful viral vector for inner ear gene therapy. Nat. Commun. *10*, 427.

35. Chien, W.W., McDougald, D.S., Roy, S., Fitzgerald, T.S., and Cunningham, L.L. (2015). Cochlear gene transfer mediated by adeno-associated virus: Comparison of two surgical approaches. Laryngoscope *125*, 2557–2564.

36. György, B., Meijer, E.J., Ivanchenko, M.V., Tenneson, K., Emond, F., Hanlon, K.S., Indzhykulian, A.A., Volak, A., Karavitaki, K.D., Tamvakologos, P.I., et al. (2018). Gene Transfer with AAV9-PHP.B Rescues Hearing in a Mouse Model of Usher Syndrome 3A and Transduces Hair Cells in a Non-human Primate. Mol. Ther. Methods Clin. Dev. *13*, 1–13.

37. Tan, F., Chu, C., Qi, J., Li, W., You, D., Li, K., Chen, X., Zhao, W., Cheng, C., Liu, X., et al. (2019). AAV-ie enables safe and efficient gene transfer to inner ear cells. Nat. Commun. *10*, 3733.

38. Lee, J., Nist-Lund, C., Solanes, P., Goldberg, H., Wu, J., Pan, B., Schneider, B.L., and Holt, J.R. (2020). Efficient viral transduction in mouse inner ear hair cells with utricle injection and AAV9-PHP.B. Hear. Res. *394*, 107882.

39. Zhong, L., Zhao, W., Wu, J., Li, B., Zolotukhin, S., Govindasamy, L., Agbandje-McKenna, M., and Srivastava, A. (2007). A dual role of EGFR protein tyrosine kinase signaling in ubiquitination of AAV2 capsids and viral second-strand DNA synthesis. Mol. Ther. *15*, 1323–1330.

40. Zhong, L., Li, B., Mah, C.S., Govindasamy, L., Agbandje-McKenna, M., Cooper, M., Herzog, R.W., Zolotukhin, I., Warrington, K.H., Jr., Weigel-Van Aken, K.A., et al. (2008). Next generation of adeno-associated virus 2 vectors: point mutations in tyrosines lead to high-efficiency transduction at lower doses. Proc. Natl. Acad. Sci. USA *105*, 7827–7832.

41. Petrs-Silva, H., Dinculescu, A., Li, Q., Min, S.-H., Chiodo, V., Pang, J.-J., Zhong, L., Zolotukhin, S., Srivastava, A., Lewin, A.S., and Hauswirth, W.W. (2009). High-efficiency transduction of the mouse retina by tyrosine-mutant AAV serotype vectors. Mol. Ther. *17*, 463–471.

42. Petrs-Silva, H., Dinculescu, A., Li, Q., Deng, W.-T., Pang, J.-J., Min, S.-H., Chiodo, V., Neeley, A.W., Govindasamy, L., Bennett, A., et al. (2011). Novel properties of tyrosine-mutant AAV2 vectors in the mouse retina. Mol. Ther. *19*, 293–301.

43. Mowat, F.M., Gornik, K.R., Dinculescu, A., Boye, S.L., Hauswirth, W.W., Petersen-Jones, S.M., and Bartoe, J.T. (2014). Tyrosine capsid-mutant AAV vectors for gene delivery to the canine retina from a subretinal or intravitreal approach. Gene Ther. *21*, 96–105.

44. Khimich, D., Nouvian, R., Pujol, R., Tom Dieck, S., Egner, A., Gundelfinger, E.D., and Moser, T. (2005). Hair cell synaptic ribbons are essential for synchronous auditory signalling. Nature *434*, 889–894.

45. Becker, L., Schnee, M.E., Niwa, M., Sun, W., Maxeiner, S., Talaei, S., Kachar, B., Rutherford, M.A., and Ricci, A.J. (2018). The presynaptic ribbon maintains vesicle populations at the hair cell afferent fiber synapse. eLife *7*, e30241.

46. El-Badry, M.M., and McFadden, S.L. (2007). Electrophysiological correlates of progressive sensorineural pathology in carboplatin-treated chinchillas. Brain Res. *1134*, 122–130.

47. Kiang, N.Y.S., Moxon, E.C., and Kahn, A.R. (1976). The relationship of gross potentials recorded from the cochlea to single unit activity in the auditory nerve. In Electrocochleography, R. Rubin, C. Elberling, and G. Salomon, eds. (University Park Press), pp. 95–115.

48. Pujol, R., Puel, J.L., Gervais d'Aldin, C., and Eybalin, M. (1993). Pathophysiology of the glutamatergic synapses in the cochlea. Acta Otolaryngol. *113*, 330–334.

49. Ruel, J., Wang, J., Rebillard, G., Eybalin, M., Lloyd, R., Pujol, R., and Puel, J.L. (2007). Physiology, pharmacology and plasticity at the inner hair cell synaptic complex. Hear. Res. *227*, 19–27.

50. Chikar, J.A., Colesa, D.J., Swiderski, D.L., Di Polo, A., Raphael, Y., and Pfingst, B.E. (2008). Over-expression of BDNF by adenovirus with concurrent electrical stimulation improves cochlear implant thresholds and survival of auditory neurons. Hear. Res. *245*, 24–34.

51. Leake, P.A., Hradek, G.T., Hetherington, A.M., and Stakhovskaya, O. (2011). Brain-derived neurotrophic factor promotes cochlear spiral ganglion cell survival and function in deafened, developing cats. J. Comp. Neurol. *519*, 1526–1545.

52. Nakaizumi, T., Kawamoto, K., Minoda, R., and Raphael, Y. (2004). Adenovirus-mediated expression of brain-derived neurotrophic factor protects spiral ganglion neurons from ototoxic damage. Audiol. Neurotol. *9*, 135–143.

53. Szobota, S., Mathur, P.D., Siegel, S., Black, K., Saragovi, H.U., and Foster, A.C. (2019). BDNF, NT-3 and Trk receptor agonist monoclonal antibodies promote neuron survival, neurite extension, and synapse restoration in rat cochlea ex vivo models relevant for hidden hearing loss. PLoS ONE *14*, e0224022.

54. Zuccotti, A., Kuhn, S., Johnson, S.L., Franz, C., Singer, W., Hecker, D., Geisler, H.S., Köpschall, I., Rohbock, K., Gutsche, K., et al. (2012). Lack of brain-derived neurotrophic factor hampers inner hair cell synapse physiology, but protects against noise-induced hearing loss. J. Neurosci. *32*, 8545–8553.

55. Lidian, A., Linder, B., Anniko, M., and Nordang, L. (2013). BDNF as otoprotectant in toxin-induced hearing loss. Acta Otolaryngol. *133*, 4–11.

56. Milon, B., Mitra, S., Song, Y., Margulies, Z., Casserly, R., Drake, V., Mong, J.A., Depireux, D.A., and Hertzano, R. (2018). The impact of biological sex on the response to noise and otoprotective therapies against acoustic injury in mice. Biol. Sex Differ. *9*, 12.

57. Ollion, J., Cochennec, J., Loll, F., Escudé, C., and Boudier, T. (2013). TANGO: a generic tool for high-throughput 3D image analysis for studying nuclear organization. Bioinformatics *29*, 1840–1841.

58. Benjamini, Y., and Hochberg, Y. (1995). Controlling the false discovery rate: a practical and powerful approach to multiple testing. J. R. Stat. Soc. B Stat. Methodol. *57*, 289–300.

59. Barr, D.J., Levy, R., Scheepers, C., and Tily, H.J. (2013). Random effects structure for confirmatory hypothesis testing: Keep it maximal. J. Mem. Lang. *68*.

60. Matuschek, H., Klieg, R., Vasishth, S., Baayen, H., and Bates, D. (2017). Balancing Type I error and power in linear mixed models. J. Mem. Lang. *94*, 305–315.